Wind load prediction on single tree with integrated approach of L-system fractal model, wind tunnel, and tree aerodynamic simulation

Cite as: AIP Advances **10**, 075202 (2020); https://doi.org/10.1063/1.5144628
Submitted: 10 January 2020 . Accepted: 09 June 2020 . Published Online: 01 July 2020

Hee Joo Poh, Woei Leong Chan, Daniel J. Wise, Chi Wan Lim, Boo Cheong Khoo, Like Gobeawan, Zhengwei Ge, Yong Eng, Jia Xin Peng, Venugopalan S. G. Raghavan, Siddharth Sunil Jadhav, Jing Lou, Y. D. Cui, Heow Pueh Lee, Daniel Christopher Burcham, Daryl Lee, Kelvin Wenhui Li, and Irene Lee

COLLECTIONS

Paper published as part of the special topic on Chemical Physics, Energy, Fluids and Plasmas, Materials Science and Mathematical Physics

F This paper was selected as Featured

AIP Advances ARTICLE scitation.org/journal/adv

Wind load prediction on single tree with integrated approach of L-system fractal model, wind tunnel, and tree aerodynamic simulation

Cite as: AIP Advances 10, 075202 (2020); doi: 10.1063/1.5144628
Submitted: 10 January 2020 • Accepted: 9 June 2020 •
Published Online: 1 July 2020

View Online Export Citation CrossMark

Hee Joo Poh,[1,a)] Woei Leong Chan,[2] Daniel J. Wise,[1] Chi Wan Lim,[1] Boo Cheong Khoo,[2] Like Gobeawan,[1] Zhengwei Ge,[1] Yong Eng,[3] Jia Xin Peng,[3] Venugopalan S. G. Raghavan,[1] Siddharth Sunil Jadhav,[2] Jing Lou,[1] Y. D. Cui,[2] Heow Pueh Lee,[3] Daniel Christopher Burcham,[4] Daryl Lee,[4] Kelvin Wenhui Li,[5] and Irene Lee[5]

AFFILIATIONS

[1] Fluid Dynamics Department, Institute of High Performance Computing, Agency for Science, Technology and Research (A∗STAR), 1 Fusionopolis Way, #16-16 Connexis, Singapore 138632

[2] Temasek Laboratories, National University of Singapore, 5A Engineering Drive 1, #02-02, Singapore 117411

[3] Department of Mechanical Engineering, National University of Singapore, 9 Engineering Drive 1, Block EA, Singapore 117575

[4] Centre for Urban Greenery and Ecology (CUGE) National Parks Board, Singapore Botanic Gardens, 1 Cluny Road, Singapore 259569

[5] Building & Research Institute, Housing and Development Board, HDB Hub, 480 Lorong 6 Toa Payoh, Singapore 310480

[a)] **Author to whom correspondence should be addressed:** pohhj@ihpc.a-star.edu.sg

ABSTRACT

In this work, we adopt the integration of the L-system fractal tree generation, 3D printed wind tunnel modeling, and computational fluid dynamics (CFD) simulation approach to model the wind effect on a single tree. We compare the agreement between CFD simulations and wind tunnel measurements of rigid branched structures resembling trees. First, fractal tree mesh models based on species growth and branching patterns are developed to represent tree species for wind–tree modeling. Subsequently, a scaled-down fractal tree is generated with 3D-printing and subjected to tunnel testing with load cell and particle image velocimetry measurement data under the wind speed of 10 m/s and 15 m/s. Finally, CFD based on Reynolds-Average Navier–Stokes (RANS) simulation with a full closure model and Large Eddy Simulation (LES) using appropriate momentum sink and turbulence source terms for the volumetric tree is carried out. We use both the volume-average porous media and the volume-splitting discretized zones (split number $10 \times 10 \times 10$) to reproduce the momentum sink effect in the numerical simulation. Three tree species, namely, *Peltophorum pterocarpum* (yellow flame), *Khaya senegalensis* (African mahogany), and *Hopea odorata* (ironwood), are tested, and a reasonable agreement of drag force prediction and velocity profiles is obtained when comparing the CFD simulation results with wind tunnel data. The RANS modeled drag force results exhibit 20% of over-prediction, while the normalized velocity profiles display a good match of velocity decay at the tree leeward sides. On the other hand, LES produces much better results with only 3% discrepancy with the experimental results. A comparison of experimental results among the tree species is also carried out. Due to the actual random wind direction, tree slenderness representation, and structural flexibility issues, the current methodology still has the limitation for validation with urban on-site measurement. Nonetheless, this integrated approach is the first step in establishing modeling tool applicability to examine the effect of the forest structure and composition on wind loads.

I. INTRODUCTION

Urban vegetation plays an important role in improving the urban landscape. Besides enhancing the aesthetics of the city, urban greenery promotes psychological wellbeing among urban dwellers,[1,2] mitigates the urban heat effect,[3–6] and improves air quality.[7–9] However, trees must withstand forces imparted by the moving wind. In areas prone to strong winds, tree failure may cause personal injury[10] or damage to the property.[11] Hence, it is important to manage trees in a way that minimizes the risk to both people and the property when trees uproot or branches break.

At present, tree risk assessment practices rely heavily on professional judgment informed by training and experience.[12] During tree risk assessment, it is essential to consider the wind loads experienced by the tree, but there is considerable uncertainty surrounding the existing approaches to estimating such loads. In combination with field experiments, numerical models may provide greater insight about the wind-induced drag acting on trees under different scenarios. Recent developments in computational fluid dynamics (CFD), experimental validation, and field studies have sought to understand the complex and dynamic wind–tree interaction, in order to estimate the aerodynamic force that the tree can endure in given locations and assess the tree management scenario and the risk of tree failure.

Developing computational models for trees is incredibly difficult due to the complex interaction between the greenery and the wind. Vegetative structures are porous; hence, flow fields through trees deviate from solids as they experience a larger drag and the wake extends further downstream. Due to the leaves in the plants, there is also a larger surface subject to skin friction.[13] Furthermore, the flexible branches induce complex fluid–structure interactions. Hence, there are several approaches to modeling this complex phenomenon, which can be classified into three main categories: roughness length, porous media, and explicit tree modeling. Roughness length is easy to implement but does not detail spatial variations of flow due to vegetation well. The most common approach is the porous media approach because it strikes a good balance between accuracy and computational expense. The CODASC database[14] along with several other studies[15–18] uses a pressure loss coefficient to characterize the inertial loss of wind through trees. Several studies also parameterize the porosity of trees using a drag coefficient and leaf area density (LAD).[19–22] Although the porous media method requires less computational power, the coefficient is assumed to be uniform along the tree height, and hence, this method cannot capture microscale variations of wind drag on the tree. Moreover, trees come in many shapes and sizes with leaves distributed unequally along its height, as shown in Fig. 1. Modeling trees as cubic regions does not yield accurate results on the microscale. Explicit tree modeling provides high accuracy but requires high computational power to mesh and simulate, which makes it impossible to implement in large urban sites. Endalew *et al.*[23] sought to draw on the advantages of explicit tree modeling and the porous media approach by introducing porous zones around tree branches to represent leaves. Yuan *et al.*[24] also developed a semi-empirical model by correlating urban density and tree geometry indices with wind speed.

Despite the complexities and challenges to estimate the actual forces that an individual tree in urban landscapes experiences, it is still fundamentally important to understand the wind effect and loading on a single tree in order to predict the aerodynamic force that the tree can endure in the given locations. Having said that, wind–tree modeling over the single complex shape of tree branch and leaf systems still poses tremendous challenges on both geometrical reconstruction[26,27] and tree aerodynamics[28] simulations. Although it is essential to include the irregular tree branch and leaf geometry for wind load prediction on urban greenery, the computational resource and cost for meshing and CFD simulation make it impossible to model every single geometrical detail.

To circumvent the above challenge, we propose an integrated approach, with L-system fractal tree generation, three-dimensional (3D) printed wind tunnel modeling, and the tree aerodynamic simulation methodology to model the wind effect on a single tree. It is novel as the tree species modeled in the wind tunnel and tree aerodynamics simulation is actually based on the tree architecture (the growth process, branching patterns, and axis morphology), statistical growth data, and field measurements. This integrated approach involves the following three work scopes:

1. species modeling to generate 3D fractal models for general tree species in Singapore.[29,30] Finite element mesh models of the trees will also be produced.
2. 3D-printing and parameter extraction from fractal tree models to produce the fractal porous media models based on the wind tunnel experimental results to establish a relation between fractal parameters and drag coefficient, C_d.[31] A 3D-printing technique will be considered to construct the tree model with complicated geometries, and a detailed wake survey of the flow over the tree model will be carried out by particle image velocimetry (PIV).
3. 3D CFD wind–tree modeling at the wind tunnel and urban landscape to develop, simulate, validate, and implement the CFD large scale wind–tree study using the tree fractal approach, with momentum sink terms[32] being modeled as functions of the tree anisotropy, Leaf Area Density (LAD) properties, and reflecting the realistic directional effects from

FIG. 1. Variety of tree shapes.[25] (Reproduced with permission from K. Krige, Tree shapes, 2018, available at https://clctreeservices.com/tree-shapes/. Copyright 2018 CLC Tree Services.)

tree heterogeneity. The CFD analysis of flow over a single fractal tree with a high fidelity Large Eddy Simulation (LES) grid-filtering turbulence model will also be investigated.[33]

II. APPROACH

Figure 2 shows the flow chart to explain the whole methodology of the integrated approach in order to model the wind effect on a single tree.

The integrated approach comprises three main modeling techniques. First, it is the generation of tree-fractal parameters. We adopt the L-system approach to generate fractal parameters of common tree species found in the urban site. Subsequently, we produce the 3D printed model of the fractal tree and add in the tree crown generator to represent the leaves. The wind tunnel experimental work is carried out for the scaled down tree with both load cell and PIV measurement. Finally, CFD analysis with both Reynolds-Average Navier–Stokes (RANS) simulation and LES is performed. The LAD and drag coefficient are obtained from the wind tunnel, while the parametric study with various tree shapes and LAD variations is also carried out. More details about the three main modeling techniques are given in Subsections II A–II C.

A. Tree geometrical fractal modeling

1. Species fractal modeling

A tree species model is generated by a fractal procedural approach[30] using L-system[34] growth rules, which we formulated based on tree species' architecture, growth, and branching patterns.[35] Three species models are generated for the wind–tree simulation, as shown in Fig. 3: *Peltophorum pterocarpum*, *Khaya senegalensis*, and *Hopea odorata*.

2. Geometry reconstruction and meshing

The procedurally generated tree model using the L-system growth rules is represented in an MTG file format, as shown in Fig. 4(a). The MTG file format lists the branches in a hierarchically based manner, with each branch representing a contiguous chain of 3D points with a thickness parameter. By parsing and reconstructing the tree skeleton in 3D, it resulted in two types of point-to-point connectivities. At tree joint locations where multiple child branches sprout from the parent branch, a joint point is connected to three or more points; see Fig. 3(b). For the rest of the points, it will either be branch points with two connectivities or end points (including the root base of the tree) with a single connection.

Branch points and end points can be modeled as a series of connected cylinders, with the cylindrical radius as specified by the thickness parameter from the MTG file point listing. The nontrivial modeling problem lies at the tree joint region, where multiple branches fuse together at a single point. The 3D tree model surface reconstruction approach from the MTG file format is detailed in the work by Lim *et al.*[36] In it, skin surfaces are used as a proxy for modeling complex tree joints.

Skin surfaces are formed using a collection of spheres. Using the joint points and their connected branch point, together with their thickness parameters, spheres are generated to form the skin

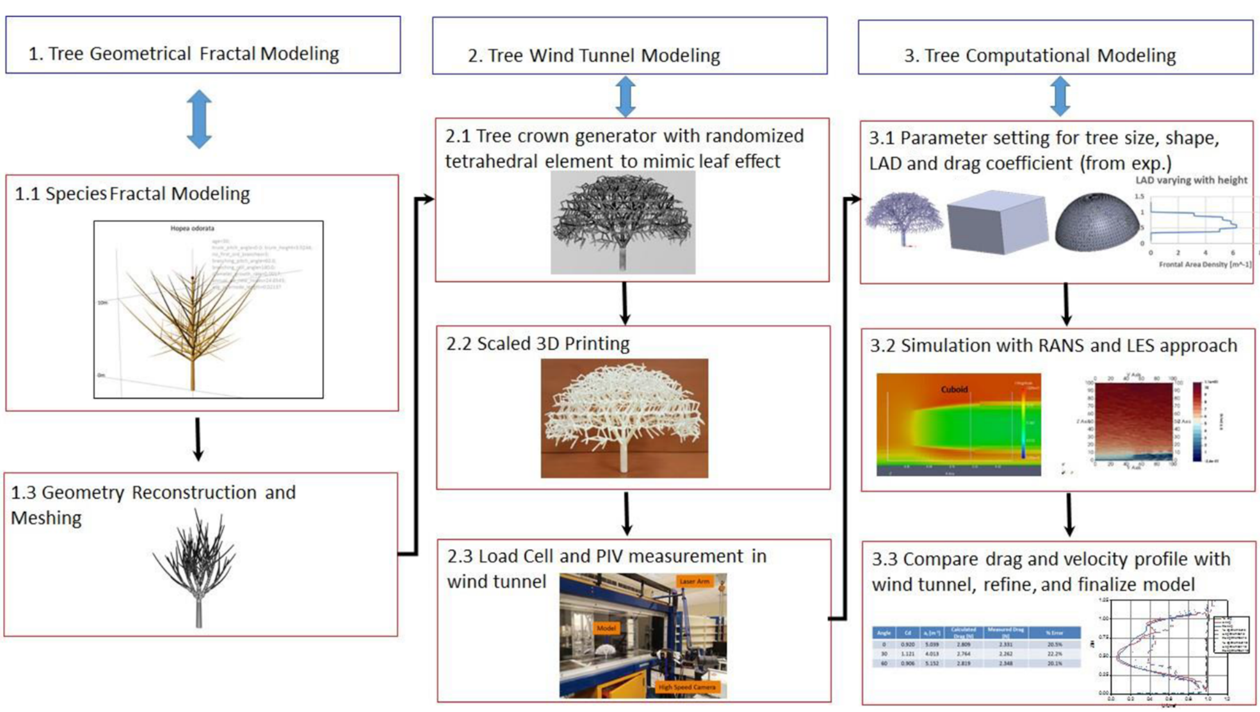

FIG. 2. Flow chart of the integrated approach to model the wind effect on a single tree.

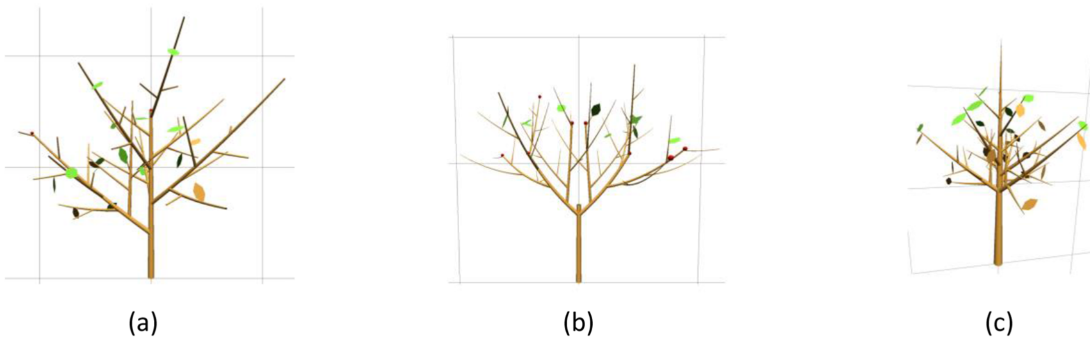

FIG. 3. Typical species models with specific growth and branching patterns, generated based on average field measurements. (a) *Peltophorum pterocarpum* (yellow flame), (b) *Khaya senegalensis* (African mahogany), (c) *Hopea odorata* (ironwood).

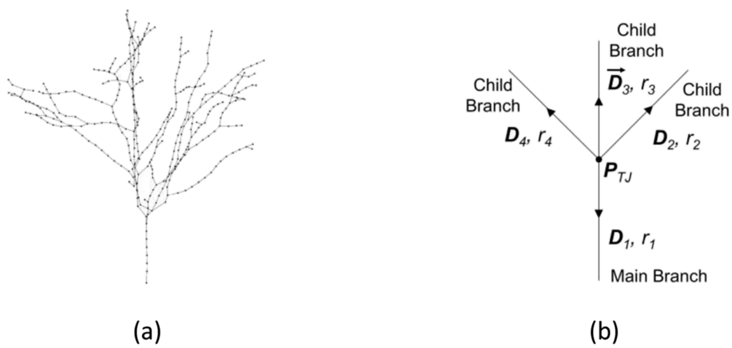

FIG. 4. The 3D representation of the MTG data. A joint point is classified as having three or more connectivities to it. (a) MTG representation in 3D, (b) closed up schematic of a joint point.

surfaces. Due to the fact that it is possible that tree joints are spaced close together, relative to their thickness, multiple tree joints can be merged together to form a bigger tree joint model; see Fig. 5. The tree joints are then meshed using the skin surface package in CGAL (Computational Geometry Algorithm Library).[37] The mesh surfaces can be refined progressively to reflect surface contours that are similar to those of trees. Subsequently, the meshes are re-meshed to improve the element quality; see Fig. 6. The final step involves the removal of half-sphere regions in order to merge with the individual branches modeled using cylindrical volumes. An example is shown in Fig. 7 for the reconstruction of the *Syzygium grande* tree species.

B. Tree wind tunnel modeling

Scaled-down 3D-printed fractal trees of 0.18 m–0.2 m height and 2 mm minimum branch diameter are produced for wind tunnel testing. The ratio of the model to actual tree is about 1:70. Due to the limitation of 3D-printing in scaled-down realistic leaves, a methodology was derived to use a porous/meshed volume to represent the tree crown. Porous volume is generated using multiple stacked and randomized tetrahedral elements. They are sized to match the frontal area ratio (the frontal silhouette area over the frontal area bounded by the tree crown shape) of the real tree, as it is discovered during the experimental stages that the frontal projected area of the crown is one of the major contributing factors to the drag force acting on the trees. The size of the tetrahedral element can be adjusted by changing the base diameter D and the sub-element diameter d, as shown in Fig. 8. Figure 9 shows the final model trees

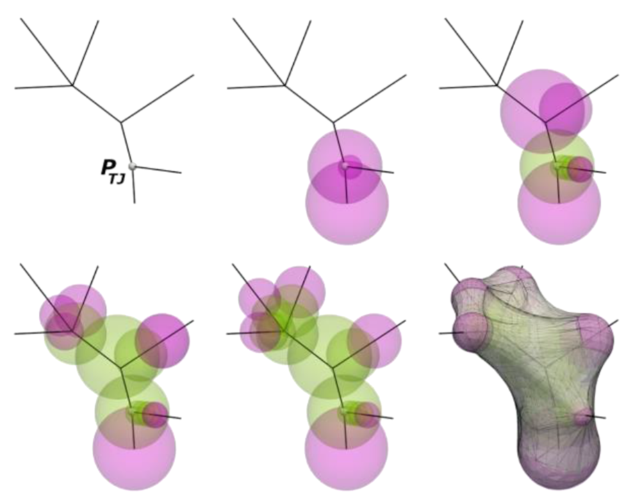

FIG. 5. Generation of a skin surface at ball joint P_{TJ} using a collection of spheres.

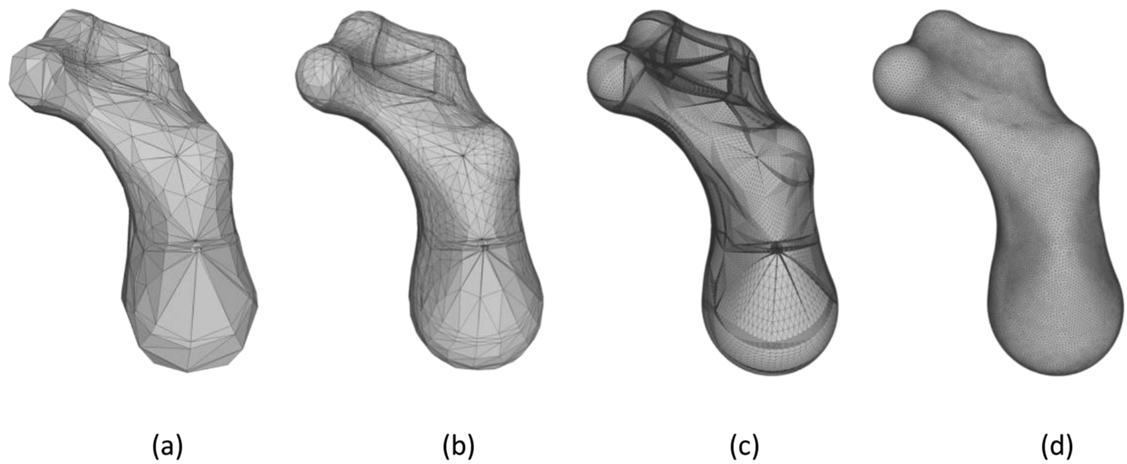

FIG. 6. Mesh generation of the tree joint surface. (a) Original meshed surface, (b) refined surface mesh, (c) further refined surface, (d) re-meshed surface mesh.

of species *Peltophorum pterocarpum*, *Khaya senegalensis*, and *Hopea odorata*. They are 3D-printed using the selective laser sintering (SLS) technique.

The wind tunnel experiment is conducted at two wind speeds, 10 m/s and 15 m/s, and different rotation angles (hence different frontal projected areas) in a closed-loop low speed wind tunnel with a test section of 0.6 (W) × 0.6 (H) × 2 m^3 (L). The tree model is mounted on the ATI gamma force balance, and the force measurement is taken for a duration of 5 s at 1000 Hz. The particle image velocimetry (PIV) system consists of a Phantom Miro M320s high speed camera, an LDY304 PIV laser, a high speed controller, a laser guiding arm, and laser sheet optics. The PIV software is LaVision DaVis 8. The turbulent intensity of the wind tunnel is between 0.2% and 0.25%, and the incoming flow is evenly distributed. PIV data are taken at the streamwise center plane for a duration of 4 s at 300 Hz. The short duration is due to instrument limitations and could incur bias in the averaged flow field. However, PIV measurements were conducted at 5 m/s, 10 m/s, and 15 m/s for each rotation angle. The averaged wake profile is shown in Fig. 10. Since the PIV measurements were started at random time and the wake profiles for each rotation angle are similar, the averaged flow field is not significantly biased.

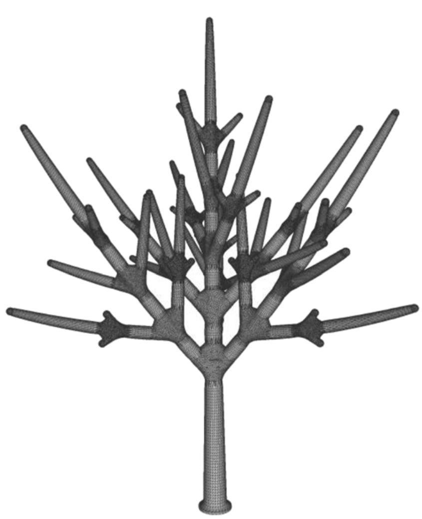

FIG. 7. Reconstructed surface mesh of the *Syzygium grande* tree species.

The wind tunnel experimental setup and testing parameters are shown in Fig. 11. The laser arm fires a laser sheet at the center plane of the tree, allowing the visualization of the flow field of the plane. Figure 11 shows the time-averaged velocity field at 10 m/s and 0° rotation for *Peltophorum pterocarpum*. The wake profile at various locations is then extracted from the velocity field (see Fig. 12).

C. Tree CFD modeling and validation

Both CFD Reynolds-Average Navier–Stokes (RANS) simulation with full closure model porous media formulation and Large Eddy Simulation (LES) with the Wall-adapting Local Eddy-viscosity (WALE) subgrid scale model are carried out for wind–tree modeling of a single tree in the wind tunnel. OpenFOAM 2.4 is used for both RANS simulation and LES analysis.

The steady state three-dimensional (3D) Reynolds-Averaged Navier–Stokes (RANS) equation is solved. The impact of the tree is modeled by a porous media approximation of the tree volume. While the trees are not explicitly modeled, additional source terms

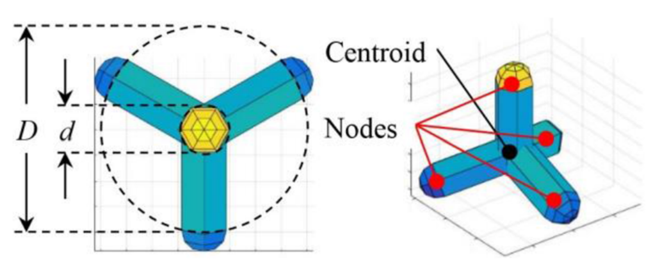

FIG. 8. Single tetrahedral element.

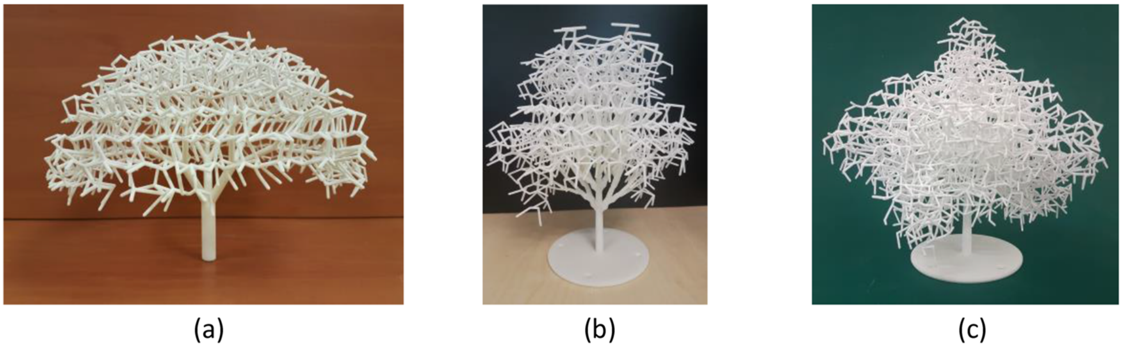

FIG. 9. Scaled-down 3D-printed tree models for wind tunnel testing. (a) *Peltophorum pterocarpum*, (b) *Khaya senegalensis*, (c) *Hopea odorata*.

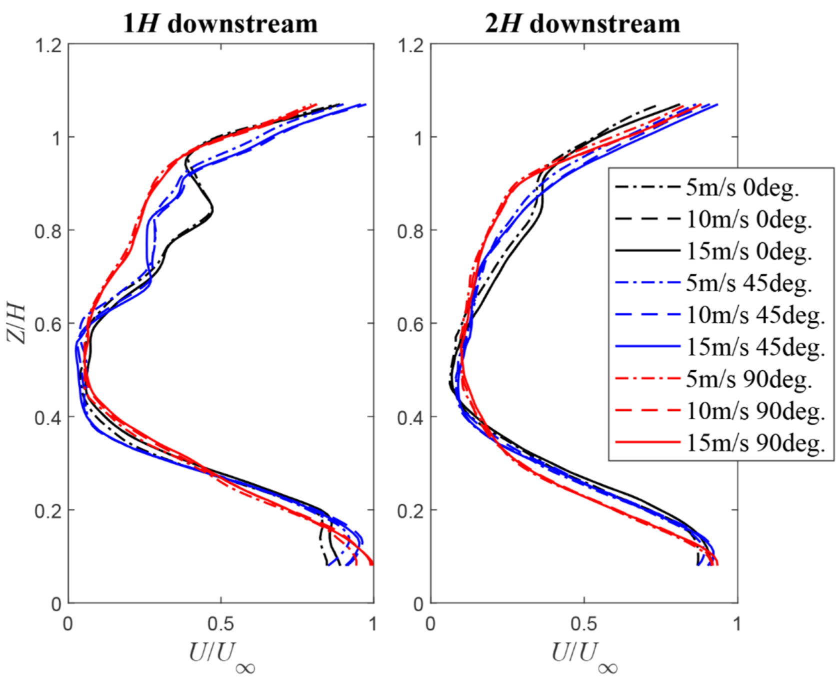

FIG. 10. Experimental measurement on the averaged wake profile of the tree model.

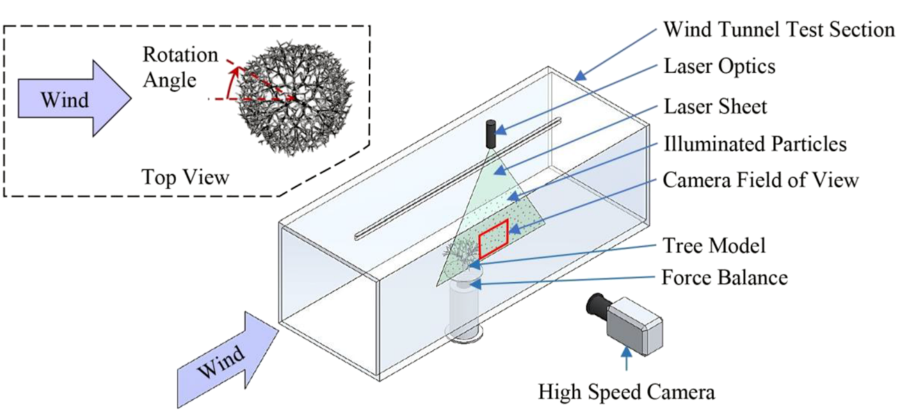

FIG. 11. Experimental setup for PIV and drag measurement.

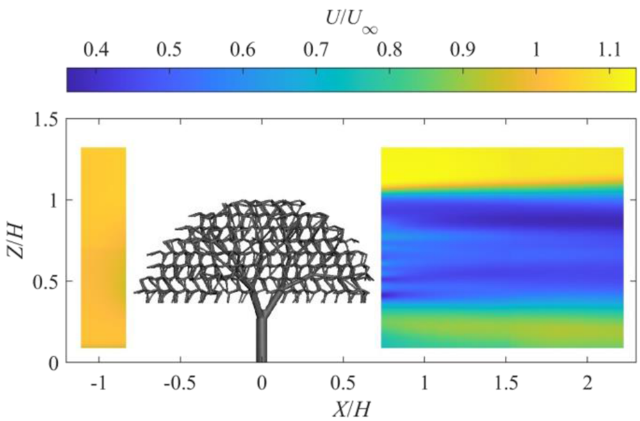

FIG. 12. Averaged velocity field at 10 m/s and 0° rotation for *Peltophorum pterocarpum*.

are introduced in the momentum equations and k-turbulence model that parameterize the aerodynamic effects from the tree volume,[38]

$$S_u = -C_d(LAD)u_i U, \tag{1}$$

$$S_k = C_d(LAD)\beta_p U^3 - C_d(LAD)\beta_d U k, \tag{2}$$

$$S_\varepsilon = C_d(LAD)\alpha_p\beta_p \frac{\varepsilon}{k} U^3 - C_d(LAD)\alpha_d\beta_d \frac{\varepsilon}{k} U k, \tag{3}$$

where S_u is the sink term added to the momentum equations, which gives the effect of trees on the velocity decrease. S_k and S_ε are the turbulence and dissipation source terms added to the transport equations of k and ε. They simulate the effects of trees on the amount of increase in turbulence and energy dissipation rate, respectively. C_d is the drag coefficient for tree canopy. LAD is the leaf area density. u_i is the velocity component. U is the velocity magnitude. α_p and α_d are the model coefficients with typical values equal to 1.5. β_p is the fraction of mean flow kinetic energy being converted to wake generated energy by the canopy drop, which has a typical value equal to 1. β_d represents the magnitude of energy losses from interactions with obstacles, which has a typical value of 4.[39]

In addition, the single fractal tree is also modeled using large eddy simulation. The incompressible Navier–Stokes equation is solved by pimpleFOAM with a wall-adapting local eddy-viscosity subgrid scale model in OpenFOAM. There are an extra source terms (S_{ui}) being added in the momentum equation which shared the same formulas as RANS. That is,

$$\frac{\partial u_i}{\partial x_i} = 0, \tag{4}$$

$$\frac{\partial u_i}{\partial t} + \frac{\partial u_i u_j}{\partial x_j} = -\frac{\partial p}{\partial x_i} + \frac{\partial}{\partial x_j}\left[\nu_t\left(\frac{\partial u_i}{\partial x_j} + \frac{\partial u_j}{\partial x_i}\right) - \frac{2}{3}\delta_{ij}k\right] + S_{ui}, \tag{5}$$

$$S_{ui} = -C_d(LAD)u_i U. \tag{6}$$

As shown in Fig. 13, the porous effect parameters adopted in this LES simulation are similar to the RANS counterpart. However, the mesh has to be finer. The mesh is 200 and 250 in stream-wise and normal directions, respectively. The first layer is 0.1 m and stretched in the normal direction. The time step is being constrained as the Courant–Friedrichs–Lewy (CFL) number should not exceed 1 for the stability purpose in density-based explicit formulation. The solver is solved in second order, and residue criteria for pressure and velocity are 10^{-6}. The simulation is initialized by the inlet profile and runs until the field data reached the statistically stable state. Consequently, the turbulence data are being collected and reached a statistically stable state.

To summarize, the volumetric tree canopy in both RANS simulation and LES is modeled using appropriate momentum sink and turbulence source terms. Momentum sink $S_u = C_d(\text{LAD})u_i U$ is added to the momentum equation in which C_d is the drag coefficient for tree canopy, LAD is the tree leaf area density (m^2/m^3), u_i is the velocity component (m/s), and U is the velocity magnitude.

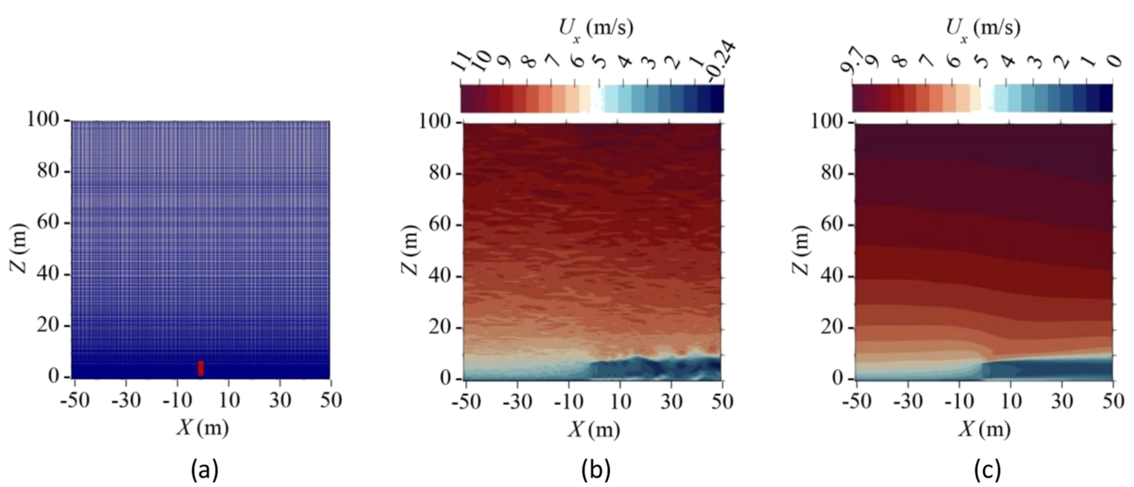

FIG. 13. (a) Mesh and porous region indicated in red. (b) Instantaneous streamwise velocity contour. (c) Time averaged streamwise velocity contour.

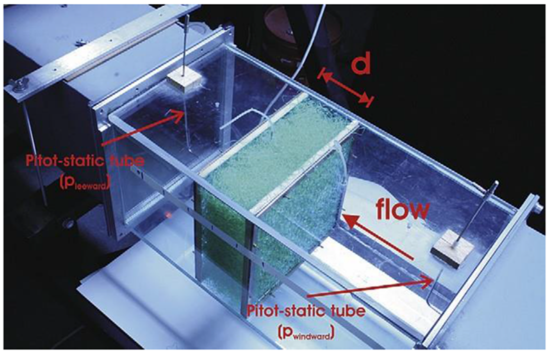

FIG. 14. Measurement for pressure loss coefficient λ in tree modeling. [Reproduced with permission from C. Gromke, Environ. Pollut. **159**, 2094–2099 (2011). Copyright 2010 Elsevier Ltd.]

For tree modeling, the product of C_d and LAD is termed the pressure loss coefficient, λ.[40] It is the parameter that describes integrated permeability and depends on the internal structure of the obstacle. Mathematically, it is the static pressure loss p_{stat} per material thickness normalized by the dynamic pressure p_{dyn} (see Fig. 14). That is,

$$\lambda = \frac{\Delta p_{stat}}{p_{dyn} d} = \frac{p_{luv} - p_{lee}}{(1/2)\rho u^2 d}, \tag{7}$$

where u is the mean velocity component in the streamwise direction, d is the obstacle's streamwise depth, p_{luv} is the static pressure windward of the obstacle, and p_{lee} is the static pressure leeward of the obstacle ρ density of the fluid.

Both the RANS and LES results are validated with the work done by Yang *et al.*[38] The experimental data measured from the windbreak test in the publications,[38] as shown in Fig. 15, are used for comparison with the computational results. An LAD value equal to 1.17 (m^{-1}) and C_d = 0.8 are adopted in the simulations, as indicated in this paper. In Sec. III, we replace it with the term Frontal Area Density (FAD) as it reflects better physical insight on tree aerodynamics analysis. Figure 16 shows the comparison of the mean velocity profiles at different locations downstream of the vegetated windbreak. The blue dots represent the experimental data measured from a field experiment of vegetated windbreak flow. The green dots represent the numerical simulation results obtained by Yang *et al.*,[38] which was performed using ANSYS-Fluent. The black broken and solid lines represent the simulation results based on our OpenFOAM tree canopy model for RANS and LES, respectively. It can be seen that the results have good agreement with experimental measurement data as well as the numerical results. The difference of the near-ground velocity between the OpenFOAM results and Yang's results could be due to the different inlet profiles and wall treatment between the two models. In the OpenFOAM model, we are using the log-law atmospheric boundary layer (ABL) conditions, as adopted in Singapore Green Building mark code,[41] while in Yang's model, a power-law inlet velocity profile was imposed on the boundary. Despite the differences, the verification work of the windbreak flow exhibited the applicability of our present OpenFOAM code in simulating the tree canopy flow with RANS and LES modeling.

III. RESULTS

A. Tree CFD modeling and comparing with wind tunnel results

Typically, for drag force calculation over the solid body, it is the summation of normal force resulting from the drag and shear force due to the friction on the surface. However, for the porous tree model, it is important to note that drag force calculation also needs to take into account the additional components due to net momentum flux. Figure 17 shows the fundamental difference for drag force calculation between the solid body and porous medium. For a rigid tree model, F_P and F_S are the forces due to wind pressure and shear friction on the tree surface and F_D is the horizontal force acting on the bottom of trunk, which is measured by the load cell. F_D is the summation of F_P and F_S. For a porous tree model, R_i and R_o are the momentum flux transferred in and out of the porous zone, F_P and F_S are the force due to the wind pressure and shear friction on the porous zone, and F_D is the drag force from the momentum sink term S_u due to the tree crown effect. The following equation [Eq. (8)] is the equation for the drag force of the porous tree model,

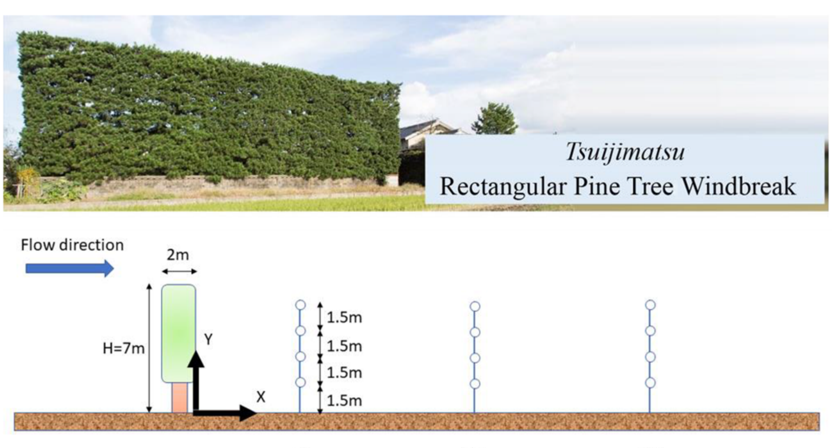

FIG. 15. Scheme of the numerical model of windbreak flow.

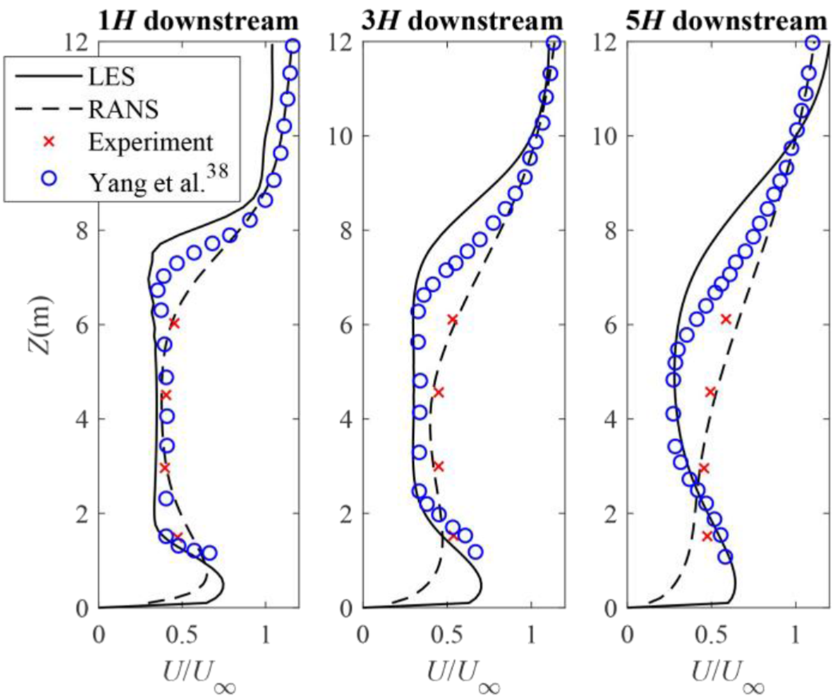

FIG. 16. Velocity profiles at different locations.

$$F_D = -\iiint \rho C_D(LAD)u_i U = R_i - R_o - F_S - F_P. \quad (8)$$

In our CFD modeling analysis, the cross section and longitudinal length of the domain are 0.6 × 0.6 × 10 m^3, which is matching the wind tunnel cross section. The tree is modeled as suspended porous media located at 65 mm above the wind tunnel, as shown in Fig. 18.

For RANS simulation, the whole domain is discretized with hexa-dominated grids with a total grid number around 4 × 10^6. "Non-slip" wall conditions are set on the walls. "Velocity inlet" conditions are applied with a constant incoming wind velocity. "Pressure" conditions with prescribed atmospheric pressure are imposed at the outlet. First, we look at the geometrical shape effect in the wind–tree modeling.

As the crown shape of the tree in the wind tunnel test is ellipsoid, while the porous tree model uses a cuboid shape, we first study the effect of the tree geometry shape on the velocity profiles and drag force. In our initial study, two geometry shapes have been analyzed: ellipsoid and cuboid (see Fig. 19). The volume, frontal area, and height of the two geometries are maintained the same and kept similar to the wind tunnel model of *Peltophorum pterocarpum*. The simulation results of velocity contours and profiles are shown in Figs. 20 and 21. It is found that the porous media model with an ellipsoid shape is not able to give the results trend consistent with the wind tunnel output, as shown in velocity profiles behind the tree. Meanwhile, we also compare the calculated drag forces on the tree from the two shapes, which are 2.860 N and 2.885 N for cuboid and ellipsoid, respectively. The difference between the two drag forces is only 0.8%, which is negligible. In view of computational domain simplicity, we will keep the cuboid shape in the following tree porous media simulations. In fact, the tree modeling with the simplification

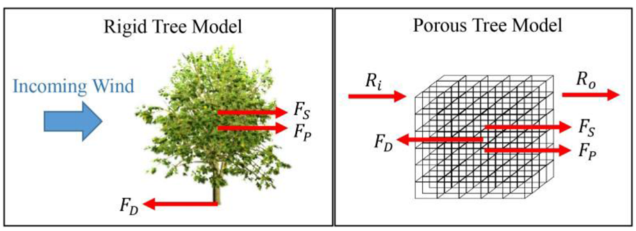

FIG. 17. Drag force calculation for the solid body and porous medium.

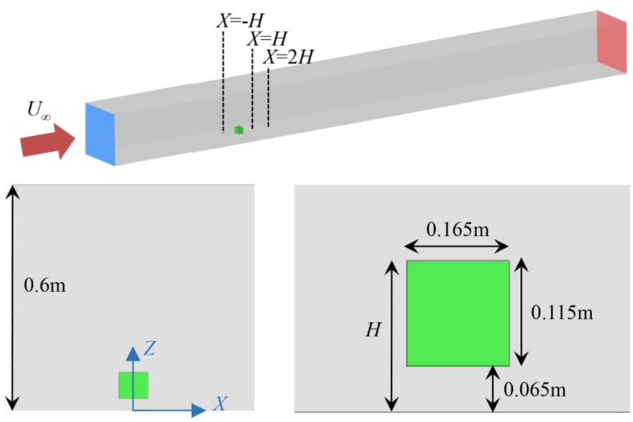

FIG. 18. Schematic of the tunnel and tree geometry.

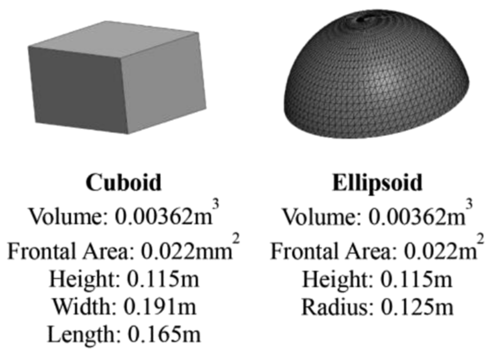

FIG. 19. Ellipsoid and cuboid used in the porous volume CFD simulation.

of canopy shapes to cuboid geometry has also been reported by the previous literature.[19]

The second parametric study is to look at the Leaf Area Density (LAD) in Eqs. (1) and (3), which is one of the important inputs derived from the experimental work for the CFD simulation. Determination of the actual value of LAD for the printed tree model is still unknown, as previous researchers used different parameters such as plant area density, which include all the surface area of the tree, leaf area density with double sides of the leaf area being taken into account, and frontal silhouette area density, with the leaf projected area being taken into account. A sensitivity study of parameter LAD is carried out to analyze the impacts of LAD on velocity profiles and drag force. In the model, we maintain the volume, frontal area, and height of cuboid the same as the tree model in the wind tunnel test. The drag coefficient is set to be 0.76 (from wind tunnel load cell measurement). A series of values of LAD varying from 0.1 to 20 have been studied. The results of velocity profiles and drag forces against LAD are shown in Figs. 22 and 23. The percentage errors between experimental and simulation results are shown in Fig. 24. The sensitivity study with LAD shows that discrepancies appear to be larger for very small and very large LADs. The value between 4 and 8 seems to produce reasonable results. With this constant LAD assumption, it would yield about 20% discrepancy when compared with wind tunnel results (either drag or average velocity comparison).

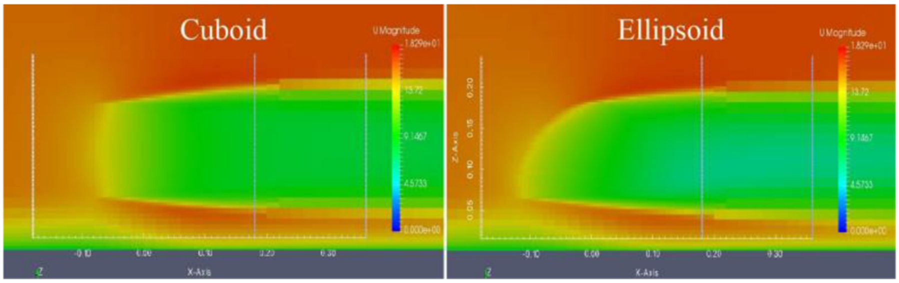

FIG. 20. Velocity contours at the vertical cutting plane around the porous tree zone.

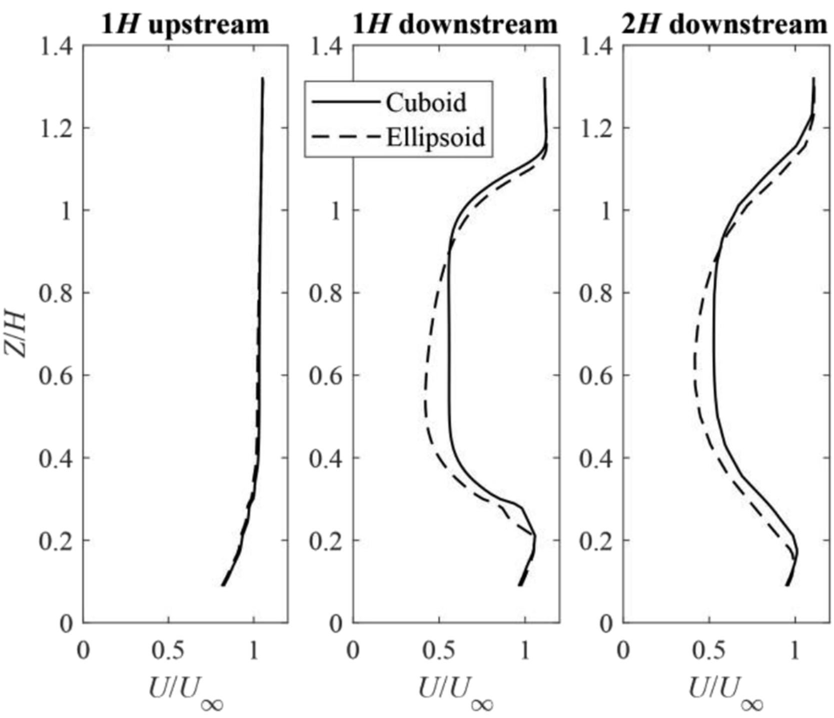

FIG. 21. Velocity profiles at different locations in the wind tunnel with 15 m/s inlet velocity.

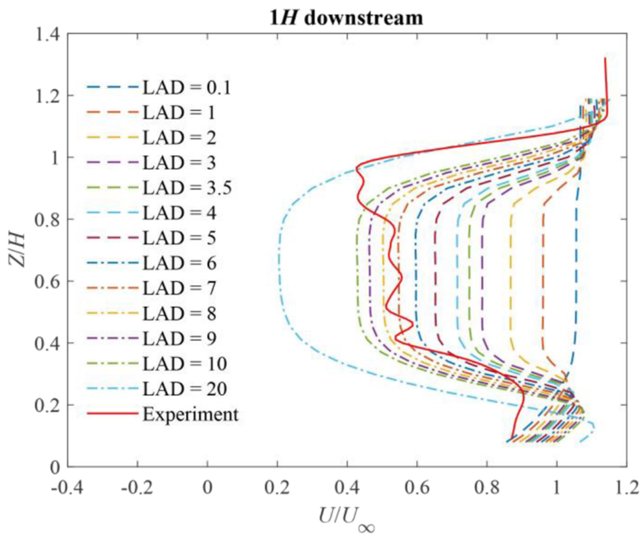

FIG. 22. Velocity profiles at $x = H$ (1*H* downstream) in the wind tunnel with 15 m/s inlet velocity.

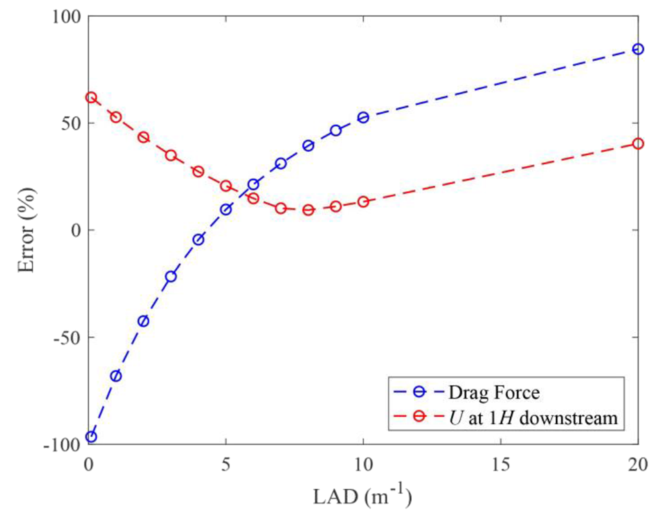

FIG. 24. Error of drag and velocity at $x = H$ against LAD.

If LAD is calculated based on the plant area density of the yellow flame tree model in the wind tunnel test, which is 11.3 m^{-1}, the drag force obtained from the CFD simulation is 3.675 N, which is about 59% different from the experimental data 2.313 N. The errors of velocity profiles are less than the drag force, which are 4.27%, 12.08%, and 11.56% for the locations $x = -H$, $x = H$, and $x = 2H$ in the wind tunnel. From the literature review, it is found that in the wind tunnel test, the frontal area density (FAD) is more commonly adopted to represent the leaf area density for the full closure model. In view of this, we calculate the frontal silhouette area density of the tree model used in the wind tunnel test, as listed in Table I.

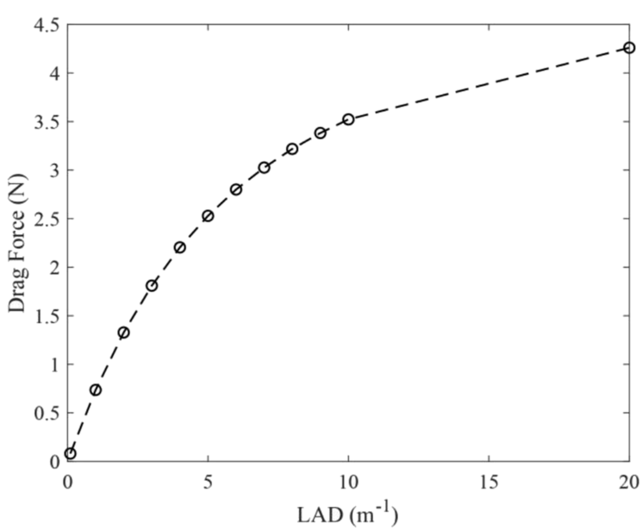

FIG. 23. Plots of drag force against LAD.

The total resultant drag coefficient, C_D, is calculated accordingly based on the frontal silhouette area, as listed in Table II.

Finally, we found that the most prior literature has used the Leaf Area Density (LAD) calculation based on the plant area density of the tree model in the wind tunnel test, and this resulted in strictly incorrect calculation, most often over-predicting drag force by more than 50%. Instead, we made the correction and proposed the frontal silhouette area of the tree model for the calculation of frontal area density (FAD) to represent the leaf area density for the full closure model. This has resulted in tremendous improvement to the CFD drag force comparison with the experimental results. With FAD = 4.375, C_d = 0.98, and a free stream velocity of 15 m/s, RANS simulation produces the drag force calculation with about +21% error. However, drastic improvement can be obtained with the LES simulation result, as it yields only +2.95% error when compared with the experimental data. The comparison of the results is summarized in Table III.

Figures 25 and 26 show the velocity profile comparison between the wind tunnel experiment and simulation for both RANS and LES results, for *Peltophorum pterocarpum* and *Khaya senegalensis* tree models, respectively. Both porous tree modeling approaches use the volume-average method. From the

TABLE I. Model tree crown parameters of *Peltophorum pterocarpum*.

Peltophorum pterocarpum			
Crown volume (m^3)		0.003 323	
Rotation angle (deg)	0	30	60
Frontal projected area (m^2)	0.016 65	0.013 36	0.016 49
FAD (m^{-1})	5.012 2	4.020 6	4.963 6

TABLE II. Total resultant drag coefficient calculated from the crown projected area and frontal silhouette area.

		Crown projected area		Frontal silhouette projected area	
V (m/s)	Rotation angle (deg)	A (m^2)	C_D	A (m^2)	C_D
15	0	0.022	0.770	0.0184	0.920
15	30	0.022	0.755	0.0146	1.121
15	60	0.022	0.775	0.0188	0.906

TABLE III. CFD results' comparison with experimental data on drag force for the case study with FAD = 4.375, C_d = 0.98, and a free stream velocity of 15 m/s.

Wind tunnel load cell measured drag force (N)	Calculated drag force with RANS simulation (N)	Error (%)	Calculated drag force with LES simulation (N)	Error (%)
2.314	2.797	+20.9	2.382	+2.95

downstream velocity profile comparison, it was found that the volume average porous media modeling approach is not able to give good matching of velocity decay with the experimental results, especially for the highly anisotropic tree crown of the Khaya tree.

In view of the above limitation, we propose a more refined modeling approach with volume-splitting discretized zones to reproduce the fine-grained heterogeneous momentum sink effect of the single tree canopy. The porous canopy zone is further discretized by 5 and 10 in *X*, *Y*, and *Z* directions, which results in 5^3 and 10^3 elements, respectively (see Fig. 27). The fifth and tenth slices for slice number 10 are shown in Figs. 27(c) and 27(d). The frontal area density (FAD) of each element is defined as the ratio between the frontal silhouette area in the streamwise direction and individual element's

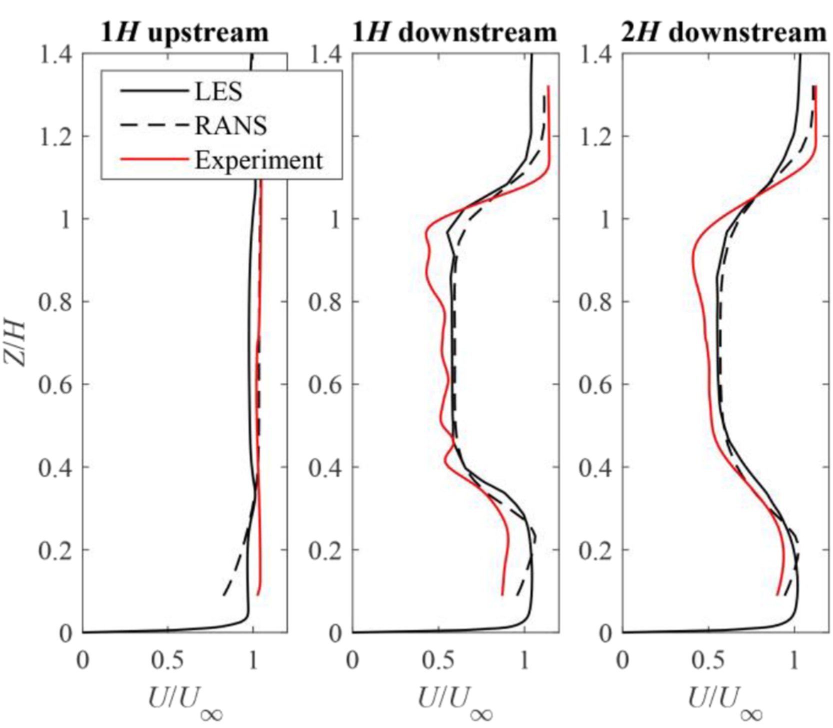

FIG. 25. Comparison of simulated and experimental velocity profiles for *Peltophorum pterocarpum* at 0° rotation.

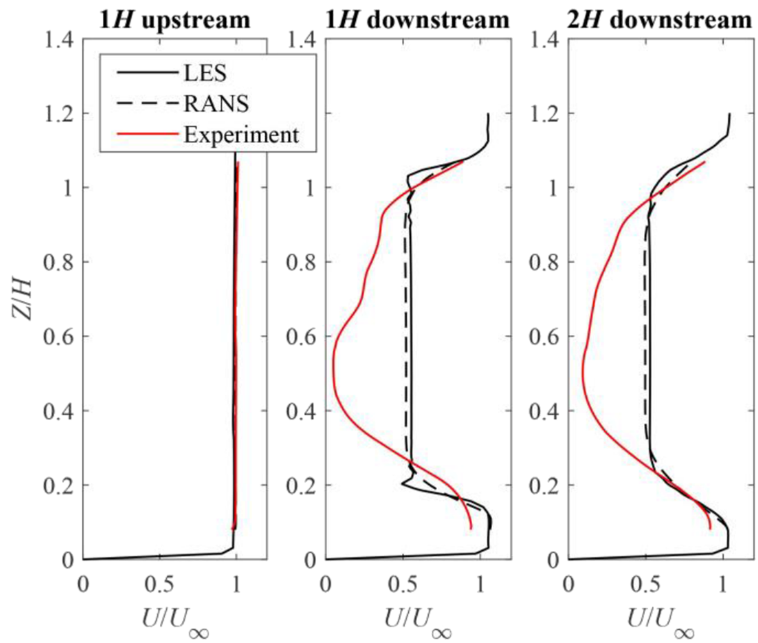

FIG. 26. Comparison of simulated and experimental velocity profiles for *Khaya senegalensis* at 0° rotation.

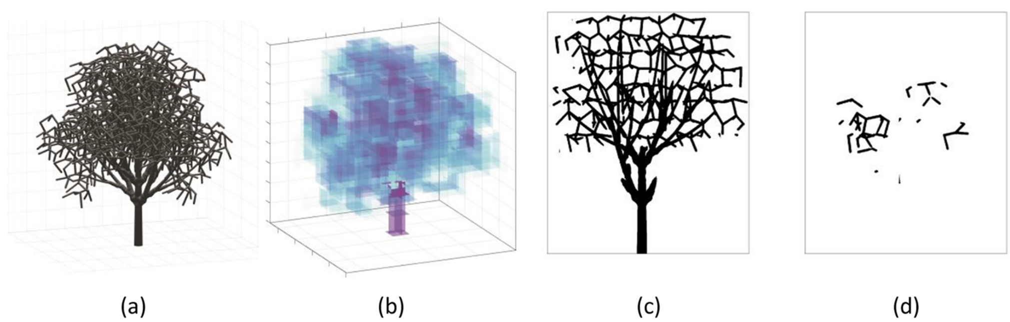

FIG. 27. (a) Khaya fractal model, (b) discretized frontal silhouette area density (contains 10^3 elements), (c) slice no. 7 (near the trunk), and (d) slice no. 10 (near to the leeward side).

volume. The resultant discretized FAD elements were implemented in LES.

The LES simulations are carried out by manipulating the drag coefficient (C_d) value from 0.1 to 0.9. This C_d value is implemented in the momentum sink term (S_{ui}) to represent the tree model. As shown in Fig. 28, the drag obtained from split numbers 5 and 10 has a similar profile as the C_d varies. The simulations with C_d = 0.4 are further compared with PIV measurement from the experiment at $x = -H$, $x = H$, and $x = 2H$ (Fig. 29). The velocity profile becomes stratified in cases with a split number of 5 due to its lower momentum sink resolution. On the other hand, the velocity profile of the wake has better agreement in the case with a split number of 10. The velocity deficit in trunk's region ($z/H < 0.2$) is also well captured. These indicate that the discretized momentum sink's resolution plays an important role in the accuracy of velocity profiles.

The calculated drag for C_d = 0.4 is presented in Table IV. The calculated drag's error has significant improvement (+1.6%)

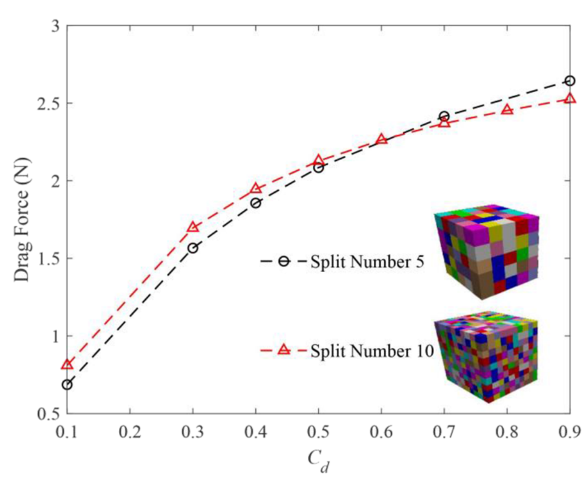

FIG. 28. Predicted drag on the tree with different discretization resolutions.

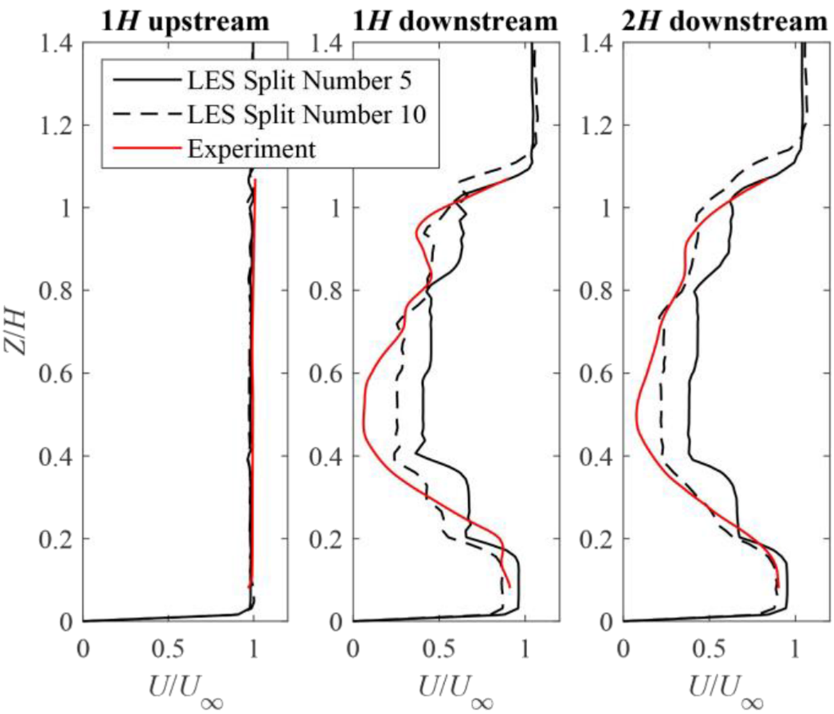

FIG. 29. Velocity profiles in the wake region (C_d = 0.4).

compared with the volume averaged momentum sink (+11.37%) method. This error decreases as the resolution increased.

B. Drag comparison between the tree species

Table V shows the model tree crown parameters of the scaled-down tree models of *Peltophorum pterocarpum*, *Khaya senegalensis*, and *Hopea odorata*.

It is observed that the frontal projected (or silhouette) area for *Khaya senegalensis* is generally lower than that for *Peltophorum pterocarpum*. However, *Khaya senegalensis* has higher FAD due to the smaller crown volume. As for *Hopea odorata*, it has the highest frontal projected area, with quite moderate crown volume when compared with the other two species, hence resulting in the average value of FAD among the three species.

Figure 30 shows the comparison of the total resultant drag coefficient, C_D, measured in the wind tunnel for the three tree species. *Khaya senegalensis* gives a lower C_D value despite the higher FAD geometrical data. Conversely, *Peltophorum pterocarpum* which has the lowest FAD gives the highest C_D. It also shows that C_D is closely correlated with FAD. Since FAD is the reciprocal of the effective depth of the tree crown, the smaller the FAD, the deeper the crown, and the larger the C_D.

TABLE IV. LES calculated drag prediction on the model tree.

Case	Drag (N)	Drag error (%)	Velocity error at H (%)
Experimental	1.9154	...	...
Split number = 5	1.856	−3.1	30.1
Split number = 10	1.945	1.6	17.4

TABLE V. Model tree crown parameters of *Peltophorum pterocarpum*, *Khaya senegalensis*, and *Hopea odorata*.

Peltophorum pterocarpum			
Crown volume (m^3)		0.003 323	
Rotation angle (deg)	0	30	60
Frontal projected area (m^2)	0.016 65	0.013 36	0.016 49
FAD (m^{-1})	5.012 2	4.020 6	4.963 6
Khaya senegalensis			
Crown volume (m^3)		0.001 861	
Rotation angle (deg)	0	45	90
Frontal projected area (m^2)	0.014 38	0.015 75	0.014 01
FAD (m^{-1})	7.726 9	8.464 8	7.529 1
Hopea odorata			
Crown volume (m^3)		0.002 708	
Rotation angle (deg)	0	45	90
Frontal projected area (m^2)	0.019 24	0.019 36	0.018 33
FAD (m^{-1})	7.105 8	7.150 5	6.768 5

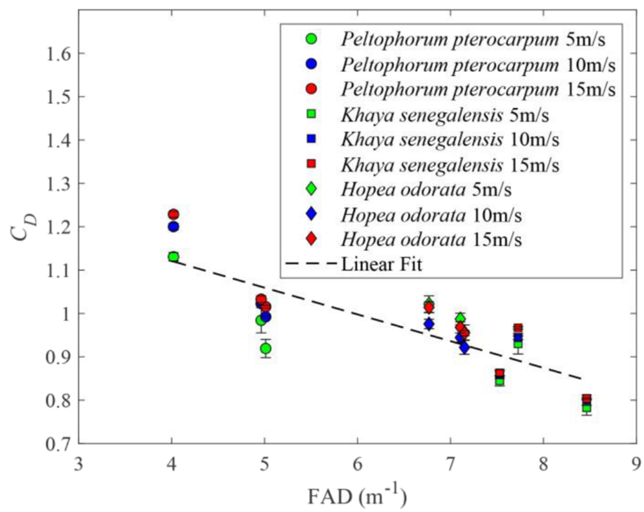

FIG. 30. C_D comparison for different tree species.

IV. CONCLUSIONS

A possibly first of its kind approach using the integration of L-system fractal tree generation, 3D printed wind tunnel modeling, and the CFD simulation methodology to model the wind effect on a single tree and predict the tree drag force has been proposed and analyzed. This integrated approach uses species modeling based on tree species growth and branching patterns to generate 3D fractal tree models, which were meshed and downscale printed (70:1) for wind tunnel PIV and drag force measurement, and employs both RANS simulation and LES for CFD flow modeling and drag calculation for further validation. Testing has been carried out for the yellow flame tree, and RANS produces a reasonable prediction of 80% accuracy for drag force prediction. The higher fidelity of LES turbulence modeling gives a much better accuracy of 97%, better drag estimates than RANS, albeit at the expense of computational cost. It is also confirmed that the improved numerical estimates using a discretized momentum source in simulations can yield much better results than the volume average momentum source. However, this methodology has a limitation for the actual size tree model due to scaling issues and inherits complexities of urban on-site measurements. In addition, it is found that the Frontal Area Density (FAD) value using the frontal silhouette area of the tree model is of paramount importance for CFD tree modeling and gives the insightful information about tree permeability and the pressure loss coefficient. Experimental results for species *Peltophorum pterocarpum*, *Khaya senegalensis*, and *Hopea odorata* also reveal that there could be intrinsic correlation between the pressure loss coefficient (λ) with drag force and velocity decay downstream for the wind effect on tree and vegetation. In the future, sensitivity analysis with a CFD parametric study associated with other tree species [e.g., *Samanea saman* (rain tree) and *Syzygium grande* (sea apple)] for model improvement as well as the extension to the site of 1×1 km^2 of the computational domain with the greenery of individual tree species distribution, a layout of a mixed array of buildings, and an undulating terrain will be performed to capture the wind loading on trees in the urban landscape.

ACKNOWLEDGMENTS

The authors gratefully acknowledge the financial support of the research (Grant No. NRF2017VSG-AT3DCM001-029) from the National Research Foundation of Singapore.

DATA AVAILABILITY

The data that support the findings of this study are available from the corresponding author upon reasonable request.

REFERENCES

[1] J. Mennis, M. Mason, and A. Ambrus, "Urban greenspace is associated with reduced psychological stress among adolescents: A Geographic Ecological Momentary Assessment (GEMA) analysis of activity space," Landscape Urban Plann. **174**, 1–9 (2018).

[2] M. S. Taylor, B. W. Wheeler, M. P. White, T. Economou, and N. J. Osborne, "Research note: Urban street tree density and antidepressant prescription rates—A cross-sectional study in London, UK," Landscape Urban Plann. **136**, 174–179 (2015).

[3] E. Ng, L. Chen, Y. Wang, and C. Yuan, "A study on the cooling effects of greening in a high-density city: An experience from Hong Kong," Build. Environ. **47**, 256–271 (2012).

[4] L. Kong *et al.*, "Regulation of outdoor thermal comfort by trees in Hong Kong," Sustainable Cities Soc. **31**, 12–25 (2017).

[5] A. M. Coutts, E. C. White, N. J. Tapper, J. Beringer, and S. J. Livesley, "Temperature and human thermal comfort effects of street trees across three contrasting street canyon environments," Theor. Appl. Climatol. **124**(1), 55–68 (2016).

[6] D. Chen, X. Wang, M. Thatcher, G. Barnett, A. Kachenko, and R. Prince, "Urban vegetation for reducing heat related mortality," Environ. Pollut. **192**, 275–284 (2014).

[7] D. J. Nowak, D. E. Crane, and J. C. Stevens, "Air pollution removal by urban trees and shrubs in the United States," Urban For. Urban Greening **4**(3), 115–123 (2006).

[8] D. J. Nowak, S. Hirabayashi, M. Doyle, M. McGovern, and J. Pasher, "Air pollution removal by urban forests in Canada and its effect on air quality and human health," Urban For. Urban Greening **29**, 40–48 (2018).

[9] L. Chen, C. Liu, R. Zou, M. Yang, and Z. Zhang, "Experimental examination of effectiveness of vegetation as bio-filter of particulate matters in the urban environment," Environ. Pollut. **208**, 198–208 (2016).

[10] T. W. Schmidlin, "Human fatalities from wind-related tree failures in the United States, 1995–2007," Nat. Hazards **50**(1), 13–25 (2009) (in English).

[11] M. A. van Haaften, M. P. M. Meuwissen, C. Gardebroek, and J. Kopinga, "Trends in financial damage related to urban tree failure in The Netherlands," Urban For. Urban Greening **15**, 15–21 (2016).

[12] A. K. Koeser and E. T. Smiley, "Impact of assessor on tree risk assessment ratings and prescribed mitigation measures," Urban For. Urban Greening **24**, 109–115 (2017).

[13] C. Gromke and B. Ruck, "Aerodynamic modelling of trees for small-scale wind tunnel studies," Forestry **81**(3), 243–258 (2008).

[14] C. Gromke, R. Buccolieri, S. Di Sabatino, and B. Ruck, "Dispersion study in a street canyon with tree planting by means of wind tunnel and numerical investigations—Evaluation of CFD data with experimental data," Atmos. Environ. **42**(37), 8640–8650 (2008).

[15] R. Buccolieri, C. Gromke, S. Di Sabatino, and B. Ruck, "Aerodynamic effects of trees on pollutant concentration in street canyons," Sci. Total Environ. **407**(19), 5247–5256 (2009).

[16] R. Buccolieri *et al.*, "Analysis of local scale tree–atmosphere interaction on pollutant concentration in idealized street canyons and application to a real urban junction," Atmos. Environ. **45**(9), 1702–1713 (2011).

[17] A. P. R. Jeanjean, G. Hinchliffe, W. A. McMullan, P. S. Monks, and R. J. Leigh, "A CFD study on the effectiveness of trees to disperse road traffic emissions at a city scale," Atmos. Environ. **120**, 1–14 (2015).
[18] A. P. R. Jeanjean, R. Buccolieri, J. Eddy, P. S. Monks, and R. J. Leigh, "Air quality affected by trees in real street canyons: The case of Marylebone neighbourhood in central London," Urban For. Urban Greening **22**, 41–53 (2017).
[19] L. Liang, L. Xiaofeng, L. Borong, and Z. Yingxin, "Improved k–ε two-equation turbulence model for canopy flow," Atmos. Environ. **40**, 762–770 (2006).
[20] A. Mochida, Y. Tabata, T. Iwata, and H. Yoshino, "Examining tree canopy models for CFD prediction of wind environment at pedestrian level," J. Wind Eng. Ind. Aerodyn. **96**(10), 1667–1677 (2008).
[21] C. Gromke, B. Blocken, W. Janssen, B. Merema, T. van Hooff, and H. Timmermans, "CFD analysis of transpirational cooling by vegetation: Case study for specific meteorological conditions during a heat wave in Arnhem, Netherlands," Build. Environ. **83**, 11–26 (2015).
[22] M. Bruse and H. Fleer, "Simulating surface–plant–air interactions inside urban environments with a three dimensional numerical model," Environ. Modell. Software **13**(3), 373–384 (1998).
[23] A. M. Endalew *et al.*, "Modelling airflow within model plant canopies using an integrated approach," Comput. Electron. Agric. **66**(1), 9–24 (2009).
[24] C. Yuan, L. Norford, and E. Ng, "A semi-empirical model for the effect of trees on the urban wind environment," Landscape Urban Plann. **168**, 84–93 (2017).
[25] K. Krige, Tree shapes, 2018, available at https://clctreeservices.com/tree-shapes/.
[26] R. Zhang, Y. Zhang, K. P. Lam, and D. H. Archer, "A prototype mesh generation tool for CFD simulations in architecture domain," Build. Environ. **45**, 2253–2262 (2010).
[27] S. Hong, I. Lee, H. Hwang, I. Seo, J. Bitog, K. Kwon, J. Song, O. Moon, K. Kim, and H. Ko, "CFD modelling of livestock odour dispersion over complex terrain, Part I: Topographical modelling," Biosyst. Eng. **108**, 253–264 (2011).
[28] J. Finnigan, "Turbulence in plant canopies," Annu. Rev. Fluid Mech. **32**, 519–571 (2000).
[29] L. Gobeawan, E. S. Lin, A. Tandon, A. T. K. Yee, V. H. S. Khoo, S. N. Teo, S. Yi, C. W. Lim, S. T. Wong, D. J. Wise, P. Cheng, S. C. Liew, X. Huang, Q. H. Li, L. S. Teo, G. S. Fekete, and M. T. Poto, "Modeling trees for virtual Singapore: From data acquisition to CityGML models," Int. Arch. Photogramm., Remote Sens. Spat. Inf. Sci. **XLII-4/W10**, 55–62 (2018).
[30] L. Gobeawan, D. J. Wise, A. T. K. Yee, S. T. Wong, C. Lim, E. S. Lin, and Y. Su, in Computer Graphics International Conference, CGI 2019: Advances in Computer Graphics, 2019.
[31] A. M. Endalew, M. Hertog, M. A. Delele, K. Baetens, T. Persoons, M. Baelmans, H. Ramon, B. M. Nicolaï, and P. Verboven, "CFD modelling and wind tunnel validation of airflow through plant canopies using 3D canopy architecture," Int. J. Heat Fluid Flow. **30**(2), 356–368 (2009).
[32] J. Liu, J. M. Chen, T. A. Black, and M. D. Novak, "E-ε modelling of turbulent air flow downwind of a model forest edge," Boundary-Layer Meteorol. **77**(1), 21–44 (1996).
[33] M. G. Giometto, A. Christen, P. E. Egli, M. F. Schmid, R. T. Tooke, N. C. Coops, and M. B. Parlange, "Effects of trees on mean wind, turbulence and momentum exchange within and above a real urban environment," Adv. Water Resour. **106**, 154–168 (2017).
[34] P. Prusinkiewicz and A. Lindenmayer, *The Algorithmic Beauty of Plants* (Springer-Verlag, Berlin, Heidelberg, 1996).
[35] D. Barthélémy and Y. Caraglio, Ann. Bot. **99**, 375 (2007).
[36] C. Lim, L. Gobeawan, S. Wong, D. Wise, P. Cheng, H. Poh, and Y. Su, "Generation of tree surface mesh models from point clouds using skin surfaces," in *Proceedings of the 15th International Joint Conference on Computer Vision, Imaging and Computer Graphics Theory and Applications: Volume 1: GRAPP* (Science and Technology Publication, 2020), pp. 83–92, ISBN: 978-989-758-402-2.
[37] CGAL, *CGAL User and Reference Manual*, 4th ed. (CGAL Editorial Board, 2019).
[38] Y. Yang, Z. Xie, T. K. T. Tse, X. Jin, and M. Gu, "Verification of a tree canopy model and an example of its application in wind environment optimization," Wind Struct. Int. J. **15**, 409–421 (2012).
[39] A. Sogachev and O. Panferov, "Modification of two-equation models to account for plant drag," Boundary-Layer Meteorol. **121**, 229–266 (2006).
[40] C. Gromke, "A vegetation modeling concept for building and environmental aerodynamics wind tunnel tests and its application in pollutant dispersion studies," Environ. Pollut. **159**, 2094–2099 (2011).
[41] See https://www.bca.gov.sg/GreenMark/others/GM_NRB2015_Technical_Guide_Requirements_R3.pdf for BCA Non Residential Buildings NRB: 2015: Technical Guide and Requirements; accessed 22 October 2018.